

See discussions, stats, and author profiles for this publication at: <https://www.researchgate.net/publication/230673078>

Facile Fabrication of 3D-Ordered Macroporous Nanocrystalline Iron Oxide Films with Highly Efficient Visible Light Induced Photocatalytic Activity

ARTICLE *in* THE JOURNAL OF PHYSICAL CHEMISTRY C · JUNE 2010

Impact Factor: 4.77 · DOI: 10.1021/jp102525y

CITATIONS

51

READS

51

5 AUTHORS, INCLUDING:



Yuanzhi Li

Wuhan University of Technology

60 PUBLICATIONS 1,989 CITATIONS

[SEE PROFILE](#)



Xuijian Zhao

Wuhan University of Technology

461 PUBLICATIONS 7,347 CITATIONS

[SEE PROFILE](#)

Facile Fabrication of 3D-Ordered Macroporous Nanocrystalline Iron Oxide Films with Highly Efficient Visible Light Induced Photocatalytic Activity

Hao Xie, Yuanzhi Li,* Shaofen Jin, Jianjun Han, and Xujian Zhao

Key Laboratory of Silicate Materials Science and Engineering, Wuhan University of Technology, Ministry of Education, 122 Luoshi Road, Wuhan 430070, China

Received: March 20, 2010; Revised Manuscript Received: April 23, 2010

A facile approach of layer-by-layer depositing and hydrolysis of FeCl_3 is developed to fabricate 3D-ordered Fe_2O_3 film. The 3D-ordered Fe_2O_3 film was characterized by SEM, XRD, and DRUV-vis. It has 3D-ordered interconnecting macropores (340 nm) with nanocrystalline hematite Fe_2O_3 walls (27.2 nm). The 3D-ordered macroporous nanocrystalline Fe_2O_3 film exhibits 2.4 times larger photocatalytic activity for the photodegradation of dye in the presence of H_2O_2 under visible irradiation than the nanocrystalline $\alpha\text{-Fe}_2\text{O}_3$ film without macropores and very good photostability. The much higher photocatalytic activity of the 3D-ordered macroporous nanocrystalline Fe_2O_3 film than that of the reference Fe_2O_3 film is attributed to the unique nanostructure and architecture of the 3D-ordered Fe_2O_3 film, which result in the much greater light harvesting efficiency and efficient mass transport in the former than in the latter due to the existence of 3D-ordered interconnecting macropores. The effect of photonic stop band on the photocatalytic activity of the 3D-ordered Fe_2O_3 film was studied by angle-dependent solid-state photodegradation experiments with monochromatic irradiation. A slow photon enhancement of photocatalytic activity was achieved by adjusting the red edge of the photonic stop band of the 3D-ordered Fe_2O_3 film close to the electronic bandgap of Fe_2O_3 . The photodegradation mechanism of crystal violet on the 3D-ordered Fe_2O_3 photocatalyst in the presence or absence of H_2O_2 was discussed.

Introduction

Hematite ($\alpha\text{-Fe}_2\text{O}_3$), which is an abundant, inexpensive, and environmentally benign n-type semiconductor with a relatively narrow bandgap (2.2 eV), sufficient to utilize ~40% of the incident sunlight, has been extensively studied because of its potential applications in fields of photocatalysis,^{1,2} gas sensors,³ lithium ion battery,⁴ etc. Various nanostructured/microstructured $\alpha\text{-Fe}_2\text{O}_3$ with diverse morphologies such as nanoparticles,⁵ nanorods or nanowires,⁶ nanotubes,⁷ quasicubic,⁸ nanobelt,⁹ nanorings,¹⁰ and hollow spheres¹¹ have been prepared. Their properties are highly depended on their special structures and morphologies, and some of nano/microstructured $\alpha\text{-Fe}_2\text{O}_3$ exhibited unique properties compared with microscale $\alpha\text{-Fe}_2\text{O}_3$. For example, Jain et al.⁵ reported that the electrochemical properties of nanocrystalline $\alpha\text{-Fe}_2\text{O}_3$ were dramatically superior to those of microscale $\alpha\text{-Fe}_2\text{O}_3$ with high specific capacity of 200–250 mA g⁻¹ and good reversibility. Sun et al.^{7b} found that $\alpha\text{-Fe}_2\text{O}_3$ nanotube exhibited high sensitivity and selectivity to H_2S . Yu et al.^{11a} reported that Fe_2O_3 hollow spheres exhibited a good visible-light photocatalytic activity for the photocatalytic decolorization of RhB in the presence of H_2O_2 . It is still a great challenge and interesting topic to search for unique functions or optimize the properties of $\alpha\text{-Fe}_2\text{O}_3$ by tuning its size, morphology, dimensionality, architecture, etc.

Three-dimensionally (3D) ordered materials such as synthetic opals and inverse opal have attracted extensive interests as photonic materials.¹² Their well-defined and ordered macropores, especially in inverse opal, which connect each other through necks, provide very nice channels that can minimize tortuosity and enhance mass transport. This architecture characteristics,

which can avoid depletion region or concentration gradients, have proved to be very important and efficient to chemical separation,¹³ heterogeneous catalysis,¹⁴ and electrochemical aspect.¹⁵ On the other hand, multiple scattering and slow photons due to the significantly reduced group velocity of light near the red edge of photonic stop band found in photonic crystal greatly improve the light harvesting efficiency.¹⁶ These architecture characteristics of inverse opal are especially useful for designing highly efficient photoelectrochemical and photocatalytic materials or devices that are very significant to solar energy utilization and environmental detoxification.¹⁷

Enlightened by the unique properties of $\alpha\text{-Fe}_2\text{O}_3$ nanocrystal and morphologic characteristics of inverse opal, we combined the advantages of nanosized $\alpha\text{-Fe}_2\text{O}_3$ and inverse opal of $\alpha\text{-Fe}_2\text{O}_3$ together and have developed in this study a facile approach for the fabrication of 3D-ordered Fe_2O_3 film with interconnecting macropores and nanocrystalline $\alpha\text{-Fe}_2\text{O}_3$ wall. It was found that the unique nanostructure and architecture of the 3D-ordered Fe_2O_3 film results in its much higher photocatalytic efficiency for the photodegradation of crystal violet than conventional nanocrystalline $\alpha\text{-Fe}_2\text{O}_3$ film.

Experimental Section

Materials. Monodispersed polystyrene spheres (2.70% solid latex, diameter 0.356 μm , standard deviation 0.014 μm) were bought from Polysciences. Reagent quality KOH, isopropanol, FeCl_3 , Fe_2O_3 , crystal violet (CV), H_2O_2 (30 wt %), poly(ethylene glycol) (M_w : 4000), and ethanol were purchased from Sinopharm Chemical Reagent Co. All of these chemicals were used without further purification.

Fabrication of Ordered Latex Films. Glass slides (1.9 \times 1.3 cm) used for the experiment were first treated with a mixture

* To whom correspondence should be addressed.

of 1.0 mol/L KOH isopropanol solution for 2 h, washed with distilled water, and finally dried by flushing nitrogen gas. The glass slide was placed on an experimental bench. 30 μL of latex dispersions was dropped on the glass slide and spread uniformly on the whole area of the slide with the tip of pipet. After the water was evaporated at ambient temperature, 3D-ordered latex film was formed on the glass slide.

Fabrication of 3D-Ordered Fe_2O_3 . The as-prepared 3D-ordered latex film was placed horizontally on an experimental bench. 50 μL of 0.025 mol/L FeCl_3 solution in ethanol was dropped on the 3D-ordered latex film. The FeCl_3 precursor was spread naturally, uniformly on the whole area of the 3D-ordered latex film, and penetrated into the matrix of the 3D-ordered latex film. After the solvent was evaporated and dried at ambient temperature, the film was transferred to an oven with controlled humidity (70%) and temperature (70 °C) for 10 min. The deposited FeCl_3 was thus hydrolyzed to $\text{Fe}_2\text{O}_3 \cdot x\text{H}_2\text{O}$. This process was repeated five times. The latex moiety was removed by temperature-programmed calcination in air. The sample was heated to 450 °C at a rate of 1 °C/min and kept at the temperature for 2 h. A reference Fe_2O_3 thin film without the photonic crystal structure was prepared on a glass slide by a similar procedure only without using the 3D-ordered latex film as template. The reference Fe_2O_3 film contained same amount of Fe_2O_3 (0.0005 g) as the 3D-ordered Fe_2O_3 film. Another reference Fe_2O_3 film with larger average crystalline size of $\alpha\text{-Fe}_2\text{O}_3$ was prepared as follows. The commercial Fe_2O_3 powder was calcinated at 800 °C for 4 h. Its average crystalline size is 75.5 nm as determined by Scherrer formula ($L = 0.89\lambda/\beta \cos \theta$). 0.06 g of the obtained Fe_2O_3 powder was dispersed in 60 mL of 0.38 wt % poly(ethylene glycol) ethanol solution by ultrasonication, and the same amount of the Fe_2O_3 powder (0.0005 g) was deposited on a glass substrate followed by calcination at 450 °C for 4 h to remove poly(ethylene glycol).

Characterization. Scanning electron microscopy (SEM) images were obtained by using a Hitachi S-5200 scanning electron microscope. X-ray diffraction (XRD) patterns were obtained on a Rigaku D/Max-III A X-ray diffractometer using $\text{Cu K}\alpha$ radiation. Diffusive reflectance UV-vis (DRUV-vis) absorption spectra were recorded on a Shimadzu UV-3600 spectrophotometer.

Photocatalytic Activity. The photocatalytic activity of the photocatalysts was evaluated by the photodegradation of CV. The light source was a 500 W Xe lamp. The reaction was maintained at ambient temperature. In a typical experiment, aqueous suspensions of dye (2.5 mL, 1.0×10^{-5} mol L⁻¹) were placed in a quartz cell. The photocatalyst film on the glass substrate was immersed in the dye solution. A UV cut filter, which can filter out UV light with wavelengths below 420 nm, was placed between the quartz cell and the Xe lamp. Prior to irradiation, the dye solution was kept in the dark to ensure the establishment of an adsorption/desorption equilibrium. Then, 10 μL of 30 wt % H_2O_2 was added to the solution, and the Xe lamp was turned on. At the intervals of given irradiation time, the film was taken out from the cell, and the UV-vis absorbance of the dye aqueous solution was measured to determine the dye concentration.

The solid-state monochromatic photodegradation of CV was carried out using monochromatic light irradiation (550 ± 5 nm) from the excitation light of a Shimadzu RF-5301 PC spectrometer. The intensity of monochromatic irradiation was measured with a FZ-A radiometer. 10 μL of 30 wt % H_2O_2 was added to 2.0 mL of 1.0 mmol/L crystal violet in acetone. 20 μL of the obtained solution was dropped on the film of Fe_2O_3 . After drying

at room temperature in the dark, the film was fixed on a sample holder. For angle-dependent photodegradation experiment, the film was first irradiated at the specified angle off-normal of the films for a known time and then immersed in 4 mL of ethanol to dissolve the unreacted dye. The dye concentration was determined by measuring the UV-vis absorbance of the washing.

Detection of Hydroxyl Radicals. The experimental procedure for the detection of hydroxyl radicals was as follows. The photocatalyst film on the glass substrate was immersed in a 2.5 mL of aqueous solution of 1.0×10^{-4} mol L⁻¹ terephthalic acid and 4.0×10^{-4} mol L⁻¹ NaOH in a quartz cell at ambient temperature. Then, 10 μL of 30 wt % H_2O_2 was added to the solution. A 500 W Xe lamp was used as a light source. At the intervals of given irradiation time, the film was taken out from the cell, and PL spectra of the 2-hydroxyterephthalic acid produced by the reaction between terephthalic acid and photo-generated hydroxyl radicals were recorded on a Shimadzu RF-5301 PC spectrometer using 315 nm excitation light.

Results and Discussion

Fabrication and Characterization of 3D-Ordered Fe_2O_3 Film. Usually, inverse opal was prepared by filling of the voids of opal. As the interstitial voids are connected by small channels, the challenge is to transport and deposit material into the voids without obstructing these channels. To obtain an inverse opal, the voids must be homogeneously filled; i.e., the infill materials must be contiguous. Otherwise, as soon as the template is removed, the inhomogeneous structure collapses.¹⁸ To solve the problem, several approaches such as nanocrystals sintering, electrodeposition, and chemical vapor deposition have been developed. Here, we used layer-by-layer casting of Fe_2O_3 precursor to prepare 3D-ordered Fe_2O_3 . This casting procedure is as follows. FeCl_3 ethanol solution homogeneously filled into the voids of the opal, and then ethanol evaporated under ambient condition. The deposited FeCl_3 was hydrolyzed to $\text{Fe}_2\text{O}_3 \cdot x\text{H}_2\text{O}$ under conditions of controlled humidity (70%) and temperature (70 °C). The circle of precursor depositing, solvent evaporation, and hydrolysis was repeated five times. Finally, the 3D-ordered Fe_2O_3 was obtained by removing the template by temperature-programmed calcination. Figure 1 shows SEM images of the 3D-ordered Fe_2O_3 film. As can be seen from a low-magnification image of Figure 1a, cracks in the Fe_2O_3 thin film are observed. It was observed that the starting 3D-ordered latex film has line dislocations. Latex moiety removing by calcination leads to a shrinkage of the Fe_2O_3 film along line dislocations. Figure 1b is a top view of the SEM image at a higher magnification. The top surface is composed of a closely packed, hexagonal Fe_2O_3 array. The diameter of starting 3D-ordered latex film is 356 nm. The macropore size of the obtained 3D-ordered Fe_2O_3 film is reduced to 340 nm. The calcination-induced shrinkage is estimated to be 4.5%. The well-defined and 3D-ordered macropores in the top layer of the 3D-ordered Fe_2O_3 film connect the corresponding macropores in the sublayer through the necks with an average size of 64.6 nm (Figure 1c). The average thickness of Fe_2O_3 wall in the 3D-ordered Fe_2O_3 film is 26.7 nm. A cross-section SEM image as shown in Figure 1d exhibits vertical ordering (14 layers).

Figure 2 shows the XRD patterns of the as-prepared 3D-ordered Fe_2O_3 film. The 3D-ordered Fe_2O_3 film has five diffraction peaks at 33.2°, 35.7°, 40.9°, 49.5°, and 54.1° in the amorphous background of the glass. These peaks are consistent with the diffraction of the (104), (110), (113), (024), and (116) planes of hematite Fe_2O_3 ($\alpha\text{-Fe}_2\text{O}_3$, JCPDS89-8103), respec-

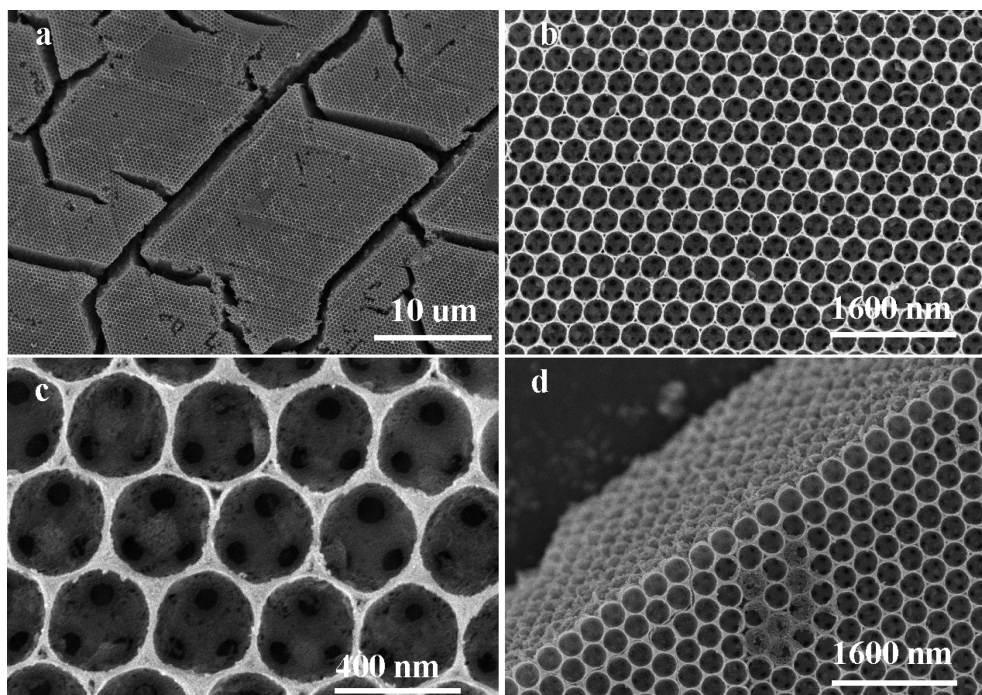


Figure 1. SEM images of the 3D-ordered Fe_2O_3 film: (a) lower magnification; (b) top view, higher magnification; (c) top view, enlarged interconnecting macropores; (d) cross-section view.

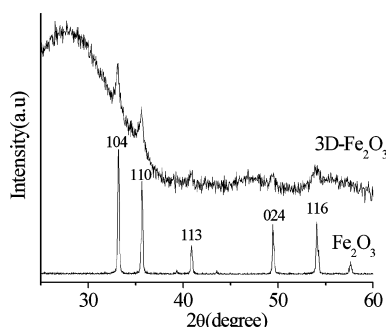


Figure 2. XRD patterns of the 3D-ordered Fe_2O_3 film and Fe_2O_3 powder with larger crystalline size.

tively. The average crystal size of $\alpha\text{-Fe}_2\text{O}_3$ in the 3D-ordered Fe_2O_3 film is determined to be 27.2 nm according to Scherrer formula, which is in agreement with the wall thickness measured by SEM. These results clearly demonstrate the formation of 3D-ordered Fe_2O_3 film with 3D-ordered interconnecting macropores and nanocrystalline $\alpha\text{-Fe}_2\text{O}_3$ walls.

Photocatalytic Activity. Effective utilization of solar light to degrade organic wastes and spent dyes in the presence of photocatalyst is expected to provide an attractive approach for environmental remediation. We chose the photodegradation of crystal violet as model dye with visible irradiation to evaluate the photocatalytic activity of the 3D-ordered Fe_2O_3 film. The intensity of the visible irradiation is $1.8 \times 10^2 \text{ mW cm}^{-2}$. Figure 3A shows the time course of the decrease in the dye concentration in the presence of H_2O_2 . CV is slowly degraded by H_2O_2 on the 3D-ordered Fe_2O_3 film in the dark. After 30 min, 40.6% of CV is degraded. Visible-light irradiation greatly accelerates the photodegradation of CV on the 3D-ordered Fe_2O_3 film. After irradiation for 30 min, 97.9% of CV is photodegraded. In contrast, compared to the highly efficient photocatalytic activity of the 3D-ordered Fe_2O_3 film, the reference Fe_2O_3 film with same average crystalline size is less efficient for the photodegradation of CV by H_2O_2 under visible irradiation. 85.6% of CV is photodegraded after irradiation for 30 min. It is well-known

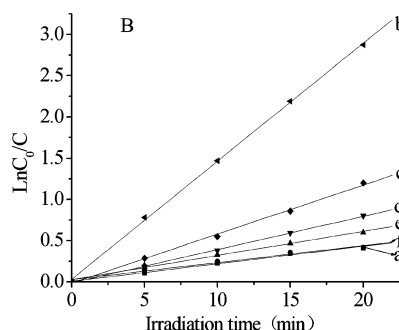
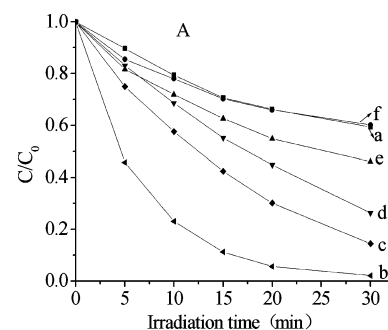


Figure 3. Time course of the decrease in the concentration (A) and $\ln(C_0/C)$ (B) for the degradation of CV with visible irradiation under different conditions: (a) the 3D-ordered Fe_2O_3 film + H_2O_2 (in dark), (b) the 3D-ordered Fe_2O_3 film + H_2O_2 , (c) the reference Fe_2O_3 film (27.2 nm) + H_2O_2 , (d) the reference Fe_2O_3 film (75.5 nm) + H_2O_2 , (e) the 3D-ordered Fe_2O_3 film, and (f) the 3D-ordered Fe_2O_3 film + CH_3OH .

that the photocatalytic degradation of dye on ferric oxide follows first-order kinetics. Figure 3B confirms that the photodegradation of CV on the photocatalysts follows first-order kinetics. The rate constant for the photodegradation of the dye on the 3D-ordered Fe_2O_3 film (0.14 min^{-1}) is 2.4 times higher than that on the reference Fe_2O_3 film. As $\alpha\text{-Fe}_2\text{O}_3$ has a short diffusion length of the photogenerated valence holes (2–20 nm),¹⁹ the

crystalline size of $\alpha\text{-Fe}_2\text{O}_3$ has a great effect on its photocatalytic and photoelectrochemical properties.²⁰ Therefore, we prepared another reference Fe_2O_3 film by depositing the same amount $\alpha\text{-Fe}_2\text{O}_3$ powder (0.0005 g) with a larger average crystalline size (75.5 nm, Figure 2) than that in the 3D-ordered Fe_2O_3 film or the above reference Fe_2O_3 film (27.2 nm) on a glass substrate and tested its photocatalytic activity for the photodegradation of CV in the presence of H_2O_2 with visible irradiation. As shown in Figure 3, the size effect of $\alpha\text{-Fe}_2\text{O}_3$ on its photocatalytic activity is quite apparent. Increasing the average crystalline size of $\alpha\text{-Fe}_2\text{O}_3$ in the reference Fe_2O_3 films from 27.2 to 75.5 nm results in the decrease of the rate constant for the photodegradation of CV from 0.059 to 0.04 min⁻¹. The rate constant for the photodegradation of CV on the 3D-ordered Fe_2O_3 film is 3.5 times higher than that on the reference Fe_2O_3 film with a larger average crystalline size (75.5 nm).

The first reference Fe_2O_3 film and the 3D-ordered Fe_2O_3 film were prepared under same procedure and experimental conditions, which results in the formation of the same amount and similar physicochemical properties (e.g., crystalline structure, crystal size, surface state, etc.) of Fe_2O_3 in the two films. The only difference among the two films is the existence of 3D-ordered macropores in the 3D-ordered Fe_2O_3 film, which does not result in an obvious increase of specific surface area. On the other hand, the sample consisting of fine powder of crushed 3D-ordered Fe_2O_3 , which was prepared by pressing the 3D-ordered Fe_2O_3 film with a stainless blade and then sonicating in water in a quartz cell to break up the inverse opal structure, has a same photodegradation rate constant as the Fe_2O_3 reference film. Therefore, the much higher photocatalytic activity of the 3D-ordered Fe_2O_3 film than the reference Fe_2O_3 film does originate from its unique 3D-ordered macroporous structure rather than their difference of physicochemical properties and surface area, as the crushed procedure cannot change its physicochemical properties and surface area.

Compared with the reference Fe_2O_3 films, the 3D-ordered interconnecting macropores in the 3D-ordered Fe_2O_3 film provide very nice channels that can minimize tortuosity and allow much more efficient mass transport for the reactant molecules to get to the photoactive sites on the Fe_2O_3 framework walls and for the product molecules to leave from the active sites to solution. This highly efficient mass transport avoids the kinetic limit of the concentration gradient caused by inefficient mass transport and thus enhances the efficiency of photodegradation in the 3D-ordered Fe_2O_3 film. Moreover, the small crystalline size of $\alpha\text{-Fe}_2\text{O}_3$ (27.2 nm) in the 3D-ordered Fe_2O_3 film avoids the disadvantage of $\alpha\text{-Fe}_2\text{O}_3$ with larger crystalline size as a visible photocatalyst due to its short diffusion length of the photogenerated valence holes and enables the photogenerated holes in bulk to efficiently transport to the surface of $\alpha\text{-Fe}_2\text{O}_3$,^{19,20} which contribute to the photodegradation of dye.

It has been reported that photocatalytic activity can be improved by enhancing light harvesting efficiency through increasing the optical path in photocatalyst with multiple scattering effect, which have been realized by preparing microstructured photocatalysts, such as Fe_2O_3 hollow microsphere^{11a} and 3D-ordered macroporous TiO_2 .^{17c} Increasing the path length of light has also been shown to improve the efficiency of dye-sensitized TiO_2 solar cells by enhancing light scattering through the incorporation of large particles and spherical voids.²¹ It is known that the optical path in a thin film of photonic crystal becomes longer due to multiple scattering when light wavelength is comparable to the periodicity of the photonic crystal.^{16b} To confirm whether the formation of 3D-

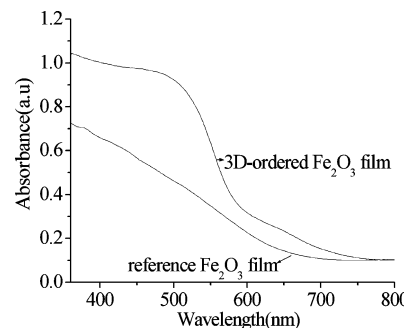


Figure 4. DRUV-vis spectra of the 3D-ordered Fe_2O_3 film and the reference Fe_2O_3 film.

ordered macropores in the 3D-ordered Fe_2O_3 film really causes enhanced light harvesting efficiency, the DRUV-vis absorption spectra of the 3D-ordered Fe_2O_3 film and the first reference Fe_2O_3 film were recorded. As shown in Figure 4, the 3D-ordered Fe_2O_3 film exhibits much stronger absorption in the region of 360–750 nm than the reference Fe_2O_3 film, which is attributed to the much longer optical path in the 3D-ordered Fe_2O_3 film as a photonic crystal with a periodicity of 340 nm than in the reference Fe_2O_3 film. The much greater light harvesting efficiency in the 3D-ordered Fe_2O_3 film than in the reference Fe_2O_3 film indicates that much more photogenerated electrons and holes are produced upon visible irradiation and thus result in the much higher photocatalytic activity in the former than in the latter.

There are two other kinds of competing effects that may affect the photocatalytic activity of the 3D-ordered Fe_2O_3 film as a photonic crystal: slow-photon enhancement at the red edge of the stop band or suppressed photoactivity due to higher reflectivity in the stop band.^{16a} According to Mihi et al.,²² the suppression due to reflectivity always dominates, as the spectral width of the stop band is argued to be much wider than the region in which enhancement due to slow photons occurs. Chen et al.^{16a} and Liu et al.²³ achieved a slow photon enhancement of photocatalytic efficiency by tuning the stop band of 3D-ordered TiO_2 to the region of the absorption tail of TiO_2 , by which the unwanted reflectivity is suppressed due to high absorption while at the same time the red edge used for enhancement still resides in a sufficiently transparent region, and then slow photon enhancement can be expected to dominate. In the present case, the 3D-ordered Fe_2O_3 film as a photonic crystal exhibits a stop band around 631 nm measured at 0° off-normal of the film (Figure 4). The spectra feature only a shoulder rather than a well-defined minimum as the energy of the stop band for the 3D-ordered Fe_2O_3 film overlaps with that of the electronic absorption band gap of Fe_2O_3 .^{16a} The experimental value of the stop band is in agreement with that of (111) planes theoretically determined by the Bragg formula²⁴

$$\lambda = \frac{2d_{hkl}}{m} \sqrt{n_{avg}^2 - \sin^2 \theta}$$

where λ is the wavelength of the stop band minimum, m is the order of Bragg diffraction, θ is the angle measured from the normal to the planes, d_{hkl} is the interplanar spacing, and n_{avg} is the average refractive index of the macroporous material ($n_{avg} = \Phi n_{walls} + (1 - \Phi)n_{voids}$, where Φ is the volume fraction of the solid wall material, n_{walls} is the refractive index of the wall material, and n_{voids} is the refractive index of the void spaces).

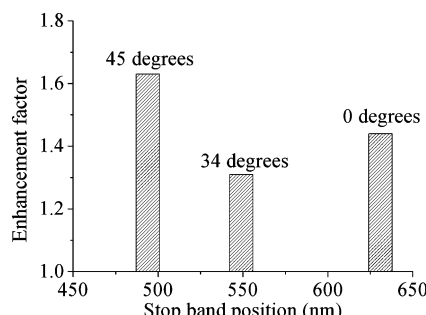


Figure 5. Photoactivity EF for the 3D-ordered Fe_2O_3 film as a function of stop band position under the monochromatic irradiation (550 nm) at the different angles off-normal of the film.

In the present photocatalytic experiment, the 3D-ordered Fe_2O_3 film was immersed in the aqueous solution of CV, and thus the stop band minimum of the 3D-ordered Fe_2O_3 film in the aqueous solution changes from 631 nm in air to 787 nm as its voids are filled by water instead of air. The stop band of the 3D-ordered Fe_2O_3 film is far away from the electronic absorption band gap of Fe_2O_3 , suggesting that neither slow photon enhancement nor suppressed photoactivity due to higher reflectivity in the stop band plays a role in the photocatalytic activity of the 3D-ordered Fe_2O_3 film.^{16a} Therefore, the great enhancement of the photocatalytic activity for the 3D-ordered Fe_2O_3 film is attributed to the much greater light harvesting efficiency in the 3D-ordered Fe_2O_3 film than in the reference Fe_2O_3 film due to the multiple scattering and efficient mass transport.

It is well-known that the effect of photonic stop band on photocatalytic activity changes with incidence angle whereas multiple scattering effects are expected to be isotropic. Angle-dependent solid-state photodegradation experiment with monochromatic irradiation was carried out to test the effect of photonic stop band on the photocatalytic activity of the 3D-ordered Fe_2O_3 film. The chosen wavelength of the monochromatic irradiation is 550 nm as it is slightly less than the electronic absorption band gap of Fe_2O_3 (2.2 eV, 561.5 nm). The intensity of the monochromatic irradiation is 4.5 mW cm⁻². In the solid state photodegradation experiment, the effects of photonic stop band and multiple scattering on the photocatalytic activity of the 3D-ordered Fe_2O_3 film can be independently studied since mass transport effects are eliminated. Figure 5 shows the photocatalytic activity of the 3D-ordered Fe_2O_3 film and the reference Fe_2O_3 film with monochromatic irradiation (550 ± 5 nm) at the different angles off-normal of the films. An enhancement factor (EF), calculated as the ratio of the decay rate constant of the 3D-ordered Fe_2O_3 film to the reference Fe_2O_3 film at the same irradiation angle off-normal of the films, was used to provide a quantitative comparison of the photodegradation.^{16b} The EF for the 3D-ordered Fe_2O_3 film to the reference Fe_2O_3 film is 1.44 at 0° off-normal. As the stop band minimum (631 nm) of the 3D-ordered Fe_2O_3 film at 0° off-normal is far away from the electronic absorption bandgap of Fe_2O_3 and the monochromatic irradiation window, the photocatalytic enhancement under the monochromatic irradiation is attributed to the multiple scattering enhancement as discussed above. Increasing the angle of incidence from 0° to 34° off-normal leads to a blue shift in the stop band from 631 to 549 nm (calculated according to the Bragg formula²⁴). The EF for the 3D-ordered Fe_2O_3 film decreases from 1.44 to 1.31, which is attributed to the suppressed photoactivity due to the higher reflectivity of the monochromatic irradiation (550 nm) in the stop band.^{16b} Further increasing the angle of incidence to 45° off-normal leads to a blue shift in the stop band to 494 nm.

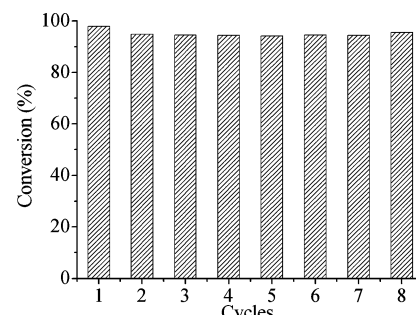


Figure 6. Durability of the 3D-ordered Fe_2O_3 film for the photodegradation of CV under visible irradiation.

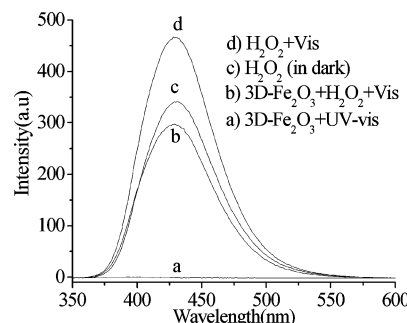


Figure 7. Fluorescence spectra of the aqueous basic solution of terephthalic acid with excitation at 315 nm under different conditions for 30 min.

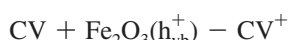
The EF for the 3D-ordered Fe_2O_3 film increases from 1.31 to 1.63. At 45° off-normal, the energy of slow photons near the red edge of the photonic stop band for the 3D-ordered Fe_2O_3 film moves into the monochromatic irradiation window.^{16b} This slow photon enhancement cause a significant increase in its photoactivity.

Photostability. The recycled experiments for the photodegradation of CV under visible irradiation were performed to evaluate the photostability of the 3D-ordered Fe_2O_3 film. As shown in Figure 6, 97.9% of CV is photodegraded when the 3D-ordered Fe_2O_3 photocatalyst is used for the first time. After successive eight cycles for the photodegradation of CV, the photocatalytic activity of the 3D-ordered Fe_2O_3 photocatalyst almost remained unchanged, indicating that the 3D-ordered Fe_2O_3 photocatalyst is photostable during the photodegradation of CV. Usually, Fe_2O_3 can be photodecomposed because of the photoreduction of Fe^{3+} to Fe^{2+} under light illumination. Once Fe^{2+} is generated, either it reacts with H_2O_2 generating OH radicals or it detaches from the oxide surface, leaving a vacancy on the oxide surface (surface dissolution). The very good photostability of the 3D-ordered Fe_2O_3 film strongly suggests that the reaction between surface Fe^{2+} and H_2O_2 is kinetically faster than the Fe^{2+} dissolution reaction in the Fe_2O_3 catalyst surface, thus preventing occurrence of catalyst photocorrosion.^{20,25}

Mechanism. To reveal the active species involved in the photodegradation process of the 3D- Fe_2O_3 photocatalyst in the absence or presence of H_2O_2 . The formation of hydroxyl radicals ($\cdot\text{OH}$) on the surface of a photocatalyst such as TiO_2 and ZnO under UV irradiation can be detected by the PL technique using terephthalic acid as a probe molecule, which readily reacts with $\cdot\text{OH}$ to produce highly fluorescent product, 2-hydroxyterephthalic acid. The PL intensity of 2-hydroxyterephthalic acid at 425 nm is proportional to the amount of $\cdot\text{OH}$ produced on the surface of the photocatalyst.²⁶ Figure 7 presents the fluorescence spectra of the aqueous basic solution of terephthalic acid with excitation at 315 nm under different conditions for 30 min. As shown in

Figure 7, in striking contrast to TiO_2 or ZnO ,²⁶ under the irradiation of UV-vis light in the absence of H_2O_2 , no detectable hydroxyl radical was probed by the PL technique using terephthalic acid as a probe molecule on the surface of the 3D- Fe_2O_3 photocatalyst. This observation suggests that the photo-generated holes on the 3D- Fe_2O_3 photocatalyst upon UV-vis irradiation do not react with hydroxyl groups to form hydroxyl radicals.

To reveal whether the active oxygen species formed by the reaction between O_2 and the photogenerated electrons contributes to the photodegradation of CV, methanol was used as hole scavenger²⁷ in the photodegradation of CV (50 mL, 1.0×10^{-4} mol L⁻¹). Figure 3 shows the time course of the decrease in the concentration of CV in the presence of excess methanol (0.99 mol L⁻¹) and the 3D- Fe_2O_3 photocatalyst under visible irradiation. As can be seen from Figure 3, although the addition of excess methanol leads to the decrease of photocatalytic activity in the absence of H_2O_2 (Figure 3e,f), CV can be slowly photodegraded with a photodegradation conversion of 39.8% within 30 min. This result suggests that CV is degraded by the active oxygen species formed by the reaction between O_2 and the photogenerated electrons. The question is: which role does the photogenerated hole on the 3D- Fe_2O_3 photocatalyst upon visible irradiation play in the photodegradation of CV? The redox potential of CV^+/CV was measured with the cyclic voltammetric method by using platinum plate and saturated $\text{Hg}_2\text{Cl}_2/\text{Hg}$ as working and reference electrodes, respectively. The potential of photoexcited CV^* and CV is -1.68 and 0.44 eV vs NHE, respectively.²⁸ As the conduction band edge and valence band edge of $\alpha\text{-Fe}_2\text{O}_3$ is 2.4 and 0.2 eV vs NHE, respectively,²⁹ the oxidation of CV by the photogenerated holes on the 3D- Fe_2O_3 photocatalyst is thermodynamically favorable:



These results suggest that the mechanism for the photodegradation of CV on the 3D- Fe_2O_3 photocatalyst in the absence of H_2O_2 is as follows: Upon visible irradiation, electrons are excited from the valence band of Fe_2O_3 to its conduction band, leaving the corresponding holes in the valence band. The photogenerated holes in the valence band of Fe_2O_3 react with CV molecules adsorbed on Fe_2O_3 to form CV^+ ions. The photogenerated electrons react with O_2 to form active oxygen species, which react with CV^+ ions and/or CV, and thus result in the photodegradation of CV.

As shown in Figure 7, in striking contrast to the above observation in the absence of H_2O_2 , after the irradiation of visible light for 30 min in the presence of H_2O_2 , a strong PL peak around 425 nm was observed for the aqueous basic solution of terephthalic acid with the 3D- Fe_2O_3 film. This observation demonstrates the production of a large amount of hydroxyl radicals in the presence of H_2O_2 and the 3D- Fe_2O_3 film upon visible irradiation. In the absence of the 3D- Fe_2O_3 photocatalyst, the solution of H_2O_2 and aqueous basic solution of terephthalic acid also exhibits a strong PL peak around 425 nm after visible irradiation for 30 min. The lower PL intensity of the solution of H_2O_2 and aqueous basic solution of terephthalic acid in the presence of the 3D- Fe_2O_3 film is attributed to the adsorption of the produced 2-hydroxyterephthalic acid on the 3D- Fe_2O_3 photocatalyst. These observations reveal that the formation of hydroxyl radicals from the decomposition of H_2O_2 has no relationship with the 3D- Fe_2O_3 photocatalyst. Actually, even in dark and in the absence of the 3D- Fe_2O_3 photocatalyst, the

solution of H_2O_2 and aqueous basic solution of terephthalic acid still exhibits a strong PL peak around 425 nm, of which the PL intensity is less than that with visible irradiation. As both H_2O_2 and terephthalic acid cannot absorb visible photons, the stronger PL intensity with visible irradiation than that in dark suggests that the thermo effect induced by the visible irradiation most probably accelerates the formation of hydroxyl radicals by the decomposition of H_2O_2 .

These results suggest that for the photodegradation of CV in the presence of H_2O_2 on the 3D- Fe_2O_3 photocatalyst there is another photodegradation pathway except for the above-mentioned photodegradation pathway in the absence of H_2O_2 as follows. CV and/or CV^+ ions, formed by the reaction between CV and the photogenerated holes in the valence band of Fe_2O_3 upon visible irradiation, react with the hydroxyl radicals formed by the decomposition of H_2O_2 , which results in the photodegradation of CV.

The much greater light harvesting efficiency in the 3D-ordered Fe_2O_3 film than in the reference Fe_2O_3 film suggests that much more photogenerated electrons and holes are produced in the former film than in the latter film upon visible irradiation, and thus much more CV^+ ions and active oxygen species are formed on the 3D-ordered Fe_2O_3 photocatalyst than on the reference Fe_2O_3 photocatalyst, which results in much higher photocatalytic efficiency of the 3D-ordered Fe_2O_3 film than that of the reference Fe_2O_3 film.

Conclusion

In summary, a facile approach was developed to fabricate 3D-ordered macroporous nanocrystalline Fe_2O_3 film. Compared with the nanocrystalline $\alpha\text{-Fe}_2\text{O}_3$ film without macropores, the 3D-ordered nanocrystalline Fe_2O_3 film exhibits enhanced photocatalytic activity for the photodegradation of dye under visible irradiation. The much higher photocatalytic activity of the 3D-ordered macroporous nanocrystalline Fe_2O_3 film than that of the nanocrystalline $\alpha\text{-Fe}_2\text{O}_3$ film is attributed to the much greater light harvesting efficiency and efficient mass transport in the former than in the latter due to the existence of 3D-ordered interconnecting macropores. A slow photon enhancement of photocatalytic activity was achieved by adjusting the red edge of photonic stop band of the 3D-ordered Fe_2O_3 film close to the electronic band gap of Fe_2O_3 . It will be possible to extend this method to fabricate a variety of 3D-ordered macroporous structures with different functionalities.

Acknowledgment. This work was supported by National Basic Research Program of China (2009CB939704), Important Project of Ministry of Education of China (309021), Scientific Research Foundation for the Returned Overseas Chinese Scholars ([2008] 890), and Nippon Sheet Glass Foundation.

References and Notes

- (1) Wang, Y. W. P.; Xu, Y. M. *Langmuir* **2009**, *25*, 2895.
- (2) Li, L. L. Y.; Chu, Y.; Liu, L.; Dong, H. *J. Phys. Chem. C* **2007**, *111*, 2123.
- (3) Wu, C. Z.; Yin, P.; Zhu, X.; Ou Yang, C. Z.; Xie, Y. *J. Phys. Chem. B* **2006**, *110*, 7806.
- (4) Zeng, S. Y.; Tang, K. B.; Li, T. W.; Liang, Z. H.; Wang, D.; Wang, Y. K.; Qi, Y. X.; Zhou, W. W. *J. Phys. Chem. C* **2008**, *112*, 4836.
- (5) Jain, G.; Balassubramanian, M.; Xu, J. *J. Mater. Sci. Mater. Mater.* **2006**, *18*, 423.
- (6) (a) Woo, K.; Lee, H. J.; Ahn, J. P.; Park, Y. S. *Adv. Mater.* **2003**, *20*, 1761. (b) Wang, X.; Chen, X.; Cao, L.; Zheng, H.; Ji, M.; Tang, C.; Sen, T.; Zhang, Z. *J. Mater. Chem.* **2004**, *14*, 905.
- (7) (a) Chen, J.; Xu, L.; Li, W. Y.; Gou, X. L. *Adv. Mater.* **2005**, *17*, 582. (b) Sun, Z. Y.; Yuan, H. Q.; Liu, Z. M.; Han, B. X.; Zhang, X. R.

- Adv. Mater.* **2005**, *17*, 2993. (c) Liu, L.; Kou, H. Z.; Mo, W. L.; Liu, H. J.; Wang, Y. Q. *J. Phys. Chem. B* **2006**, *110*, 15218.
- (8) Zheng, Y. H.; Cheng, Y.; Wang, Y. S.; Bao, F.; Zhou, L. H.; Wei, X. F.; Zhang, Y. Y.; Zheng, Q. *J. Phys. Chem. B* **2006**, *110*, 3093.
- (9) Wen, X. G.; Wang, S. H.; Ding, Y.; Wang, Z. L.; Yang, S. H. *J. Phys. Chem. B* **2005**, *109*, 215.
- (10) Jia, C. J.; Sun, L. D.; Luo, F.; Han, X. D.; Heyderman, L. J.; Yan, Z. G.; Yan, C. H.; Zheng, K.; Zhang, Z.; Takano, M.; Hayashi, N.; Eltschka, M.; Klaui, M.; Rudiger, U.; Kasama, T.; Cervera-Gontard, L.; Dunin-Borkowski, R. E.; Tzvetkov, G.; Raabe, J. *J. Am. Chem. Soc.* **2008**, *130*, 16968.
- (11) (a) Yu, J. G.; Yu, X. X.; Huang, B. B.; Zhang, X. Y.; Dai, Y. *Cryst. Growth Des.* **2009**, *9*, 1474. (b) Bang, J. H.; Suslick, K. S. *J. Am. Chem. Soc.* **2007**, *129*, 2242. (c) Cao, S. W.; Zhu, Y. J.; Ma, M. Y.; Li, L.; Zhang, L. *J. Phys. Chem. C* **2008**, *112*, 1851. (d) Zeng, S.; Tang, K.; Li, T.; Liang, Z.; Wang, D.; Wang, Y.; Zhou, W. *J. Phys. Chem. C* **2007**, *111*, 10217.
- (12) (a) Gates, B.; Xia, Y. N. *Adv. Mater.* **2001**, *13*, 1605. (b) Lopez, C. *Adv. Mater.* **2003**, *15*, 1679.
- (13) Zheng, S. P.; Ross, E.; Legg, M. A.; Wirth, M. J. *J. Am. Chem. Soc.* **2006**, *128*, 9016.
- (14) Guan, G. Q.; Zapf, R.; Kolb, G.; Men, Y.; Hessel, V.; Loewe, H.; Ye, J. H. *Chem. Commun.* **2007**, 260–262.
- (15) Sakamoto, J. S.; Dunn, B. *J. Mater. Chem.* **2002**, *12*, 2859.
- (16) (a) Chen, J. I. L.; von Freymann, G.; Choi, S. Y.; Kitaev, V.; Ozin, G. A. *Adv. Mater.* **2006**, *18*, 1915. (b) Usami, A.; Ozaki, H. *J. Phys. Chem. B* **2005**, *109*, 2591. (c) Imhof, A.; Vos, W. L.; Sprink, R.; Lagendijk, A. *Phys. Rev. Lett.* **1999**, *83*, 2942.
- (17) (a) Nishimura, S.; Abrams, N.; Lewis, B. A.; Halaoui, L. I.; Mallouk, T. E.; Benkstein, K. D.; van de Lagemaat, J.; Frank, A. J. *J. Am. Chem. Soc.* **2003**, *125*, 6306. (b) Halaoui, L. I.; Abraams, N. M.; Mallouk, T. E. *J. Phys. Chem. B* **2005**, *109*, 6334. (c) Li, Y. Z.; Kunitake, T.; Fujikawa, S. *J. Phys. Chem. B* **2006**, *110*, 13000.
- (18) Norris, D. J.; Vlasov, Y. A. *Adv. Mater.* **2001**, *13*, 371.
- (19) Kay, A.; Cesari, I.; Gratzel, M. *J. Am. Chem. Soc.* **2006**, *128*, 15714.
- (20) Wang, Y.; Du, W. P.; Xu, Y. M. *Langmuir* **2009**, *25*, 2895.
- (21) (a) Rothenberger, G.; Comte, P.; Gratzel, M. *Sol. Energy Mater. Sol. Cells* **1999**, *58*, 321. (b) Hore, S.; Nitz, P.; Vetter, C.; Prahl, C.; Niggemann, M.; Kern, R. *Chem. Commun.* **2005**, 2011.
- (22) Mihi, A.; Míguez, H. *J. Phys. Chem. B* **2005**, *109*, 15–968.
- (23) Liu, J.; Li, M. Z.; Wang, J. X.; Song, Y. L.; Jiang, L.; Murakami, T.; Fujishima, A. *Environ. Sci. Technol.* **2009**, *43*, 9425.
- (24) Schroden, R. C.; Al-Daous, M.; Blanford, C. F.; Stein, A. *Chem. Mater.* **2002**, *14*, 3305.
- (25) (a) Serpone, N.; Lawless, D.; Khairutdinov, R. *J. Phys. Chem.* **1995**, *99*, 16646. (b) Patterson, E. M.; Shelden, C. E.; Stockton, B. H. *Appl. Opt.* **1977**, *16*, 729.
- (26) (a) Yu, J. G.; Xiang, Q. J.; Zhou, M. H. *Appl. Catal., B* **2009**, *90*, 595. (b) Ishibashi, K.; Fujishima, A.; Watanabe, T.; Hashimoto, K. *Electrochem. Commun.* **2000**, *2*, 207. (c) Xiao, Q.; Si, Z. C.; Zhang, J.; Xiao, C.; Tan, X. K. *J. Hazard. Mater.* **2008**, *150*, 62. (d) Puangpatch, T.; Sreethawong, T.; Yoshikawa, S.; Chavadej, S. *J. Mol. Catal. A* **2009**, *312*, 97. (e) Ming, Y.; Chenthamarakshan, C. R.; Rajeshwar, K. *J. Photochem. Photobiol. A* **2002**, *147*, 199.
- (27) (a) Puangpatch, T.; Sreethawong, T.; Yoshikawa, S.; Chavadej, S. *J. Mol. Catal. A* **2009**, *312*, 97. (b) Ming, Y.; Chenthamarakshan, C. R.; Rajeshwar, K. *J. Photochem. Photobiol. A* **2002**, *147*, 199.
- (28) Li, Y. Z.; Zhang, H.; Hu, X. L.; Zhao, X. J.; Han, M. *J. Phys. Chem. C* **2008**, *112*, 14973.
- (29) Gondal, M. A.; Hameed, A.; Yamani, Z. H.; Suwaiyan, A. *Appl. Catal., A* **2004**, *268*, 159.

JP102525Y